Nuclear Inst. and Methods in Physics Research, A 1048 (2023) 168004

Contents lists available at ScienceDirect

Nuclear Inst. and Methods in Physics Research, A

journal homepage: www.elsevier.com/locate/nima

Technical notes

Design of beam optics for RF-separated kaon and antiproton beams in the M2 beam line of the CERN North Area

A. Gerbershagen [a,b,*], V. Andrieux [c], J. Bernhard [a], M. Brugger [a], O. Denisov [d], J. Friedrich [e], L. Gatignon [f], F. Gerigk [a], A. Guskov [g], B. Ketzer [h], F. Metzger [a,h], W.-D. Nowak [i], C. Quintans [j], S. Schuh [a]

[a] *European Organisation for Nuclear Research (CERN), Meyrin, Switzerland*
[b] *PARTREC, UMCG, University of Groningen, The Netherlands*
[c] *University of Illinois at Urbana-Champaign, Department of Physics, Urbana, USA*
[d] *National Institute for Nuclear Physics (INFN), Turin, Italy*
[e] *Technical University of Munich, Department of Physics, 85748 Garching, Germany*
[f] *Lancaster University, Physics Department, UK*
[g] *Joint Institute for Nuclear Research, Dubna, Russian Federation*
[h] *Universität Bonn, Helmholtz-Institut für Strahlen-und Kernphysik, 53115 Bonn, Germany*
[i] *Universität Mainz, Institut für Kernphysik, 55099, Germany*
[j] *LIP, 1649-003 Lisbon, Portugal*

ARTICLE INFO

Keywords:
Fixed target experiment
Kaon physics
Beamline
RF

ABSTRACT

The present contribution reviews the principle of RF separation and explains its dependence on different parameters of beam optics and hardware. The first examination of potential showstoppers for the RF-separated beam implementation for Phase-2 of the AMBER experiment in the M2 beam line of the North Area is presented. Different beam optics settings have been examined, providing either focused or parallel beams inside the RF cavities. The separation and transmission capability of the different optics settings for realistic characteristics of RF cavities are discussed and the preliminary results of the potential purity and intensity of the RF-separated beam are presented. These show that a trade-off between the overall beam intensity and the share of the required particle type in the overall beam needs to be established. No showstoppers have been identified for achieving the beam parameters required for AMBER's kaonic Primakoff reactions, kaon spectroscopy, prompt-photon production and kaon charge-radius programs. However, the high beam intensity requirements of the AMBER Drell–Yan programme cannot be satisfied with an RF-separated beam.

1. Introduction: CERN North Area

1.1. CERN accelerator complex

CERN operates a variety of beam lines and accelerators, including a number of synchrotrons, transfer lines and beams for experimental facilities. The latter include the beam lines for fixed target experiments, test beams and irradiation facilities at the CERN North Area, East Area, AD/ELENA, HiRadMat and others.

1.2. SPS extraction into the North Area

The CERN North Area receives its beam from the Super Proton Synchrotron (SPS), the second-largest synchrotron at CERN. The primary proton beam is extracted at 400 GeV/c from the SPS in 'spills', during which the beam intensity in the SPS is linearly reduced over the period of 4.8 s (slow extraction). The extraction takes place once or twice per supercycle, which has an overall duration between 25 and 60 s, depending on the scientific programme of the SPS. Prior to extraction the beam is de-bunched, so that the longitudinal distribution of the extracted particles is, in a first approximation, uniform over the period of 4.8 s.

After the extraction, the beam is split and directed towards the three North Area primary targets (T2, T4 and T6, see Fig. 1). The North Area beam lines have an overall total length of about 7 km [1]. The T6 target defines the starting point of the M2 beam line, which is with 1138 m the longest fixed-target beam line in the North Area and in the world. It transports the beam to the hall EHN2, where the AMBER [2] target and detector will be located (at the bottom right in Fig. 1).

1.3. Kaon and antiproton rates in the M2 beam line

The secondary beam in the M2 line is produced at the T6 target and transported to hall EHN2. The particle production rate depends

* Corresponding author at: European Organisation for Nuclear Research (CERN), Meyrin, Switzerland.
E-mail address: a.ge@cern.ch (A. Gerbershagen).

https://doi.org/10.1016/j.nima.2022.168004
Received 23 April 2022; Received in revised form 22 December 2022; Accepted 27 December 2022
Available online 29 December 2022

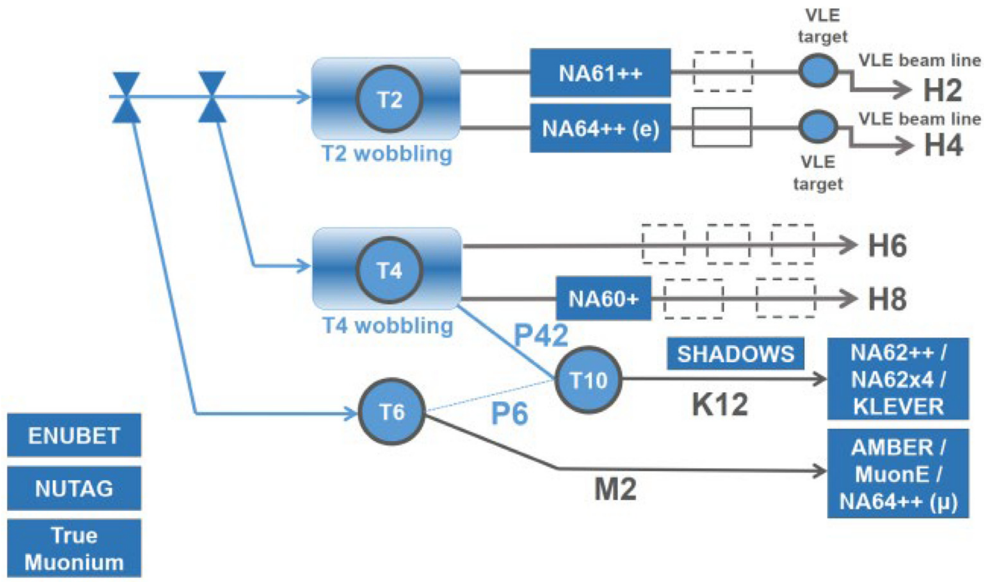

Fig. 1. Schematic diagram of the North Area beam lines (apart from TT20 tunnel) and the experiments proposed in the framework of the Physics Beyond Colliders programme. The SPS beam enters the area from the top left of the diagram.

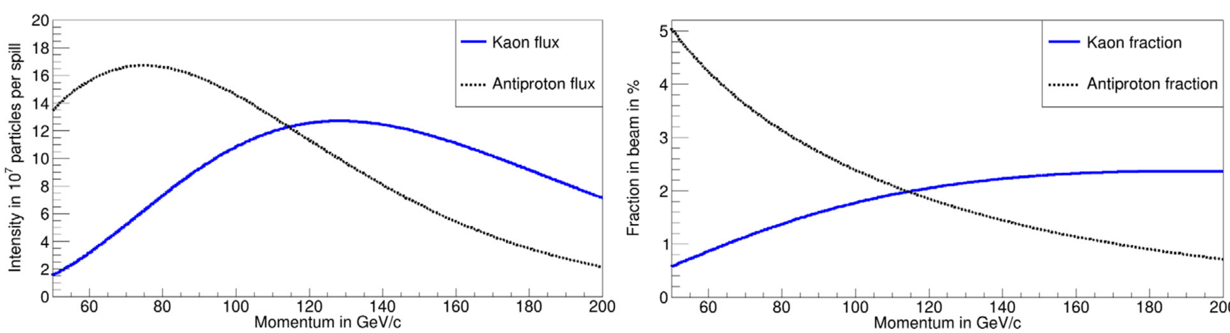

Fig. 2. Left: maximal absolute intensity of kaon and antiprotons that could be delivered per spill at the AMBER location by the M2 beam line (ignoring the constraints imposed by radiation protection). Right: share of kaons and antiprotons in the overall beam intensity.

on a number of parameters and can be described by the Atherton formula [3], which constitutes a parametrization of measured particle production data from the NA20 experiment. For the calculation of the particle rates in the present sub-section (but not in the following chapters, which are describing the RF-separated beam) the following assumptions were made:

- No particle enrichment technique is used (e.g. RF separation)
- The momentum spread has an RMS value of $\Delta p/p = 1\%$
- The (full) angular acceptance of the beam line is 17.6 mSr
- The primary particle intensity on T6 corresponds to the value currently used for the COMPASS experiment, i.e. 1.5×10^{13} protons per spill
- A Beryllium target of 500 mm length is used
- The distance from T6 to the AMBER target is the full length of M2 beam line, i.e. 1138 m
- The electrons in the secondary beam are not taken into account

Based on these assumptions and taking into consideration the kaon decay rate, the absolute rates of kaons and antiprotons per spill upon arrival in the EHN2 hall are shown in the left panel of Fig. 2 as a function of momentum. The curves show that the maximum rate for both types of particles is above 10^8 particles per spill, with the two maxima being at different momenta. However, without a purification or filtering technique applied, the fraction of those particles in the total intensity of the beam is in the order of a few percent, only (see Fig. 2, right panel).

It is important to note that there is a Radiation Protection (RP) limitation on the overall number of hadrons per spill, which can be delivered to EHN2. This limitation, given the current layout and shielding, is at approximately $4{\cdot}10^8$ particles per spill for a configuration with a hermetic absorber following the AMBER target. A new shielding configuration is being studied, which might permit to increase this value, but the increase is expected to be moderate. For a more open configuration, in which the non-interacting part of the beam continues propagation until the end of the experimental hall, the limit is at least a factor of 5 lower, depending on the detailed layout of the experiment. Hence, assuming the present overall limit on the number of hadrons and the share of the particles of interest to be below 2.5% for the 190 GeV hadron beam, at most 10^7 particles of the relevant type (kaons or antiprotons) per spill can be delivered to the hall. Additionally, the maximal rate of data acquisition and triggering systems of the AMBER experiment (and of the Cherenkov counters CEDAR detector preceding it, which serves particle identification [1]) are limited, resulting in purity rate requirements much above ~2.5%. Hence a purification needs to be considered, increasing the fraction of the relevant particles in the beam and hence permitting a sufficient intensity of the relevant particle type within the RP limitations. A number of different techniques have been examined for this purpose, such as filters of material providing differential absorption, electrostatic separation and RF separation, with the examination revealing that only the latter is capable of performing adequately at the aforementioned beam energy and intensity scales.

2. Beam requirements for Phase-2 of the AMBER experiment

The Letter of Intent for "A New QCD facility at the M2 beam line of the *CERN* SPS (AMBER)" [4] covers all ideas for future experiments as of January 2019. A detailed proposal [2] describing the measurements foreseen in AMBER Phase-1 was submitted to the CERN SPSC later in 2019 and accepted by the CERN Research Board in 2020.

Below follow short descriptions of the measurements presently envisaged for AMBER Phase-2 [5–8]. Preparatory work on the beam requirements for the AMBER Phase-2 proposal was started in 2021 by initiating first studies on the possibility to use the RF-separated beam technique in the M2 beam line [9]. A detailed description of the status of these investigations is the purpose of this work and will be given starting with the next section.

The following planned measurements, summarized in Table 1, were already discussed to some detail in the Phase-2 part of the AMBER Letter of Intent [4]. Depending on the luminosity requirements of the measurements, two configurations of the setup are considered: one comprising a hadron absorber with a beam plug located downstream of the target (so-called beam dump setup) and one where the beam crosses the full spectrometer before being dumped downstream of the apparatus (so-called open setup). The former offers a better containment of the radiation and allows for higher intensity beam while keeping compliance with radio-protection regulations. For the numbers on beam intensity it is important to distinguish between the beam intensity per spill, per second, and averaged beam intensity over a prolonged period of time. Since the spill duration is 4.8 s, the requirement on the beam intensity per spill is roughly 5 times higher than the particle rate per second during the spills. However, since the duty cycle of SPS is far below 100% due to beam extraction effects, time for machine development and SPS shutdowns, in order to estimate the beam intensity over a prolonged period of time, one needs to consider the average number of spills per hour, day etc. An approximate assumption of 2 spills per minute, 3000 spills per day of operation or $5{\cdot}10^5$ spills per calendar year can be made.

(i) Measurements of the *kaon-induced Drell–Yan (DY) reaction and charmonium production* will allow us to determine the structure of the kaon by measuring its valence, sea and gluon distributions. The two reactions are complementary: at leading order the Drell–Yan process proceeds through QED, whereas the charmonium production takes place only via QCD. Therefore, the former is sensitive to the valence and sea quarks in the kaon, whereas the later probes also its gluon distribution. As these distributions are almost completely unknown, every substantial new data is highly welcome. This is a counterpart to the pion-induced DY and charmonium measurements that were already approved for AMBER Phase-1. Analyzing both data sets together will allow for in-depth comparisons with calculational and computational QCD, e.g. on the anticipated Nambu–Goldstone nature of pion and kaon, to draw conclusions on the emergence of hadron mass.

(ii) A first measurement of the kaon polarizability via the *kaonic Primakoff* reaction K^- A→ K^- γ A would be similar to the measurement of the pion polarizability performed by COMPASS [10]. An RF-separated hadron beam, in which kaons are enriched, appears to provide a unique opportunity to perform such a measurement in one year of data taking when using a beam of 100 GeV energy with about 10^6 kaons per spill.

(iii) The *spectroscopy* of the strange-meson sector is widely uncharted territory. The goal is to identify all strange and light non-strange mesons in the quark-model multiplets and perform detailed partial wave analyses with accuracies as those successfully demonstrated by COMPASS for the $\pi^-\pi^+\pi^-$ final state [11].

(iv) Kaon-induced *prompt-photon* production is a promising way to access the quark and gluon structure of the kaon via quark–antiquark annihilation and Gluon-Compton Scattering. The proposed measurements require both positive and negative hadron beams with energies of at least 80 GeV; at this value with an intensity of the kaon component of at least $3{\cdot}10^6$ particles per spill.

(v) For completeness it should be mentioned that new interesting ideas for possible AMBER Phase 2 measurements with an RF-separated beam were brought forward recently. Here, we only mention the measurement of the charge radius of the kaon through kaon elastic scattering at low momentum transfer, e.g. at 80 GeV beam energy.

For the envisaged Phase-2 measurements with a kaon beam, except DY and charmonia measurements, an open set-up in the AMBER spectrometer will have to be used. The highest possible kaon-beam purities at moderate intensities are required, which appear to be delivered best by an RF-separated beam. The beam requirements for those AMBER Phase-2 measurements, which were already discussed in the Letter of Intent are summarized in Table 2. The beam purities given in this table include the result of kaon and pion identification as provided by Cherenkov counters (CEDARs), with numbers that are expected to be similar as it was the case for earlier COMPASS measurements (see Ref. [12]).

3. RF separated beam for M2

The RF-separation technique achieves a discrimination of particle species based on the principle that different particles have different masses and hence at the same momentum have different velocities [13, 14]. An almost monochromatic beam with a comparably narrow momentum spread of ±1% is generated by performing momentum selection in the upstream part of the beam line (see Fig. 3). Downstream of it, for the implementation of RF separation, two groups of RF cavities (with several modules each, see section 'RF Cavities & RF Power') providing a transverse kick are installed along the beam line, with the first group (RF1) reasonably close to the target and the second group (RF2) as far as possible away from the first one, in order to achieve for the different particle velocities the maximal longitudinal separation between different particle types after they traversed the distance between RF1 and RF2. Both RF1 and RF2 run at the same RF frequencies. It was assumed that the field delivering the kick in the cavities is homogeneous over the length and aperture of the cavity and has only a component deflecting the particles in the X-plane. This assumption is required for the first order simulation in MADX software [15], which can simulate only homogeneous deflection fields.

Since the primary beam extracted from the SPS and steered onto T6 is de-bunched, the secondary beam generated at the target also has an approximately constant particle flux during the 4.8 s long spill. The particles reaching RF1 receive a time-dependent transverse momentum kick by the RF cavities. It is important to note that the kick in RF1 depends only on the position of the particles along the RF phase, but not on the particle type. Then the particles propagate in the beam line towards RF2, with a velocity dependent on the particle type. There, the RF1 kick is either compensated or amplified by RF2, depending on the phase difference between RF1 and RF2. In the case of perfect kick compensation, the particles receive no overall kick from RF1 and RF2 and remain close to the beam axis. In the case of the kick not being compensated, the overall kick is non-zero (and ideally maximized), so that the particles are deflected by the sum of the phase-dependent kicks in RF1 and RF2. Hence, by modifying the frequency and relative phases of the RF cavities, the particles with a specific propagation velocity can be either chosen to remain along axis and, in the case of the specific proposed design, be absorbed by the beam dump in the beam line center, or be off-axis to circumvent the dump and be later recombined with help of the quadrupoles into a focused beam (see Fig. 3). With such an arrangement, in case of failure of the RF deflection system the full intensity of the beam is dumped in the beam dump and not transported towards the EHN2 hall, which otherwise would present a radiation danger to the personnel and could potentially damage the AMBER detector.

Table 1
Main characteristics for the Phase-2 measurements envisaged in the AMBER Letter of Intent.

	Beam dump setup		Open setup		
Name	Drell–Yan	Charmonia	Kaonic Primakoff	Spectroscopy	Prompt photons
Underlying physics	partonic structure of Kaon	partonic structure of Kaon	γ-K interaction at low-t	hadron spectroscopy	partonic structure of Kaon
Process	hard	hard	Electromagnetic	diffraction	hard
Signal	$\mu^+\mu^-$ pairs	$\mu^+\mu^-$ pairs	hard γ	charged hadrons and photons	high-p_T γ
Type of measurement	inclusive	inclusive	exclusive	exclusive	inclusive

Table 2
Beam requirements for the Phase-2 measurements envisaged in the AMBER Letter of Intent.

	Kaonic Primakoff	Spectroscopy	Prompt photons
E = 80 GeV	Perfect	Perfect	minimal possible
E = 100 GeV	Perfect	Perfect	tolerant
E = 120 GeV	Perfect	Perfect	perfect
Intensity (K) during the spill, 10^5 s^{-1}	2	4	8(80), 5(100), 4(120)
Beam sign	neg.	neg.	pos. + neg.
Beam purity, K/π after CEDARs	$>10^3$	$>10^2$	$>10^2$

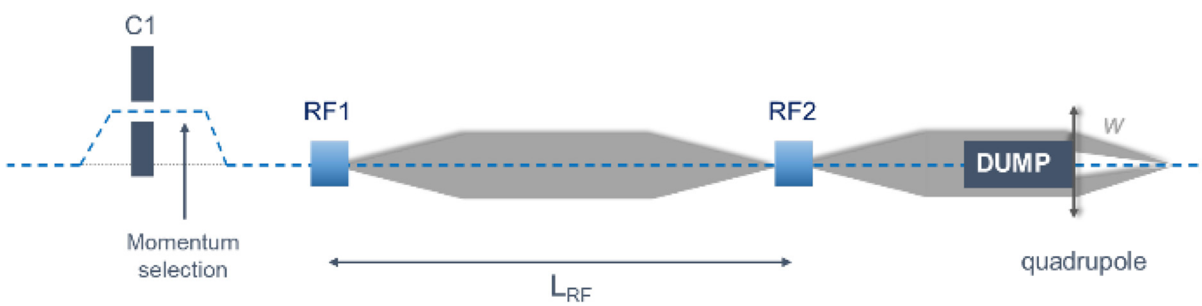

Fig. 3. Illustration of RF separated beam principle.

3.1. RF frequency and phase

The distance L between RF1 and RF2 ($L \approx 830$ m) has been maximized in the proposed design, with the first group of the cavities being located after the first group of collimators and magnets downstream of T6, and the second group with sufficient distance upstream of the AMBER target to minimize the background of particles generated (or scattered, in case of muons) at the dump to the detector. The phase difference between RF1 and RF2 for two particles with masses m_w (w for wanted) and m_u (u for unwanted) can be calculated as

$$\Delta\varphi = 2\pi f \Delta t = \frac{2\pi f L}{c} \cdot \frac{E_w - E_u}{pc} \approx \frac{\pi f L}{c} \cdot \frac{(m_w^2 - m_u^2)c^2}{p^2} \tag{1}$$

with f being the frequency of the cavities, Δt being the difference in propagation time between RF1 and RF2, E_w and E_u being the respective particle energy and p being the momentum of the particles. Eq. (1) can be reformulated to calculate the frequency required to optimally separate the two species by a given value $\Delta\varphi$:

$$f = \frac{\Delta\varphi c}{2\pi L} \cdot \frac{pc}{E_w - E_u} \approx \frac{\Delta\varphi c}{\pi L} \cdot \frac{p^2}{(m_w^2 - m_u^2)c^2} \tag{2}$$

The formula implies that there is a specific optimal frequency required to maximally separate two particle types with respective masses m_w and $m_.$. For the case of AMBER, the particles of interest are (a) positively and negatively charged kaons and (b) antiprotons. Pions and protons are the particles that one intends to filter out. The respective phase differences as a function of beam momentum and RF frequency are shown in Fig. 4. Both the purification of the kaon beam and of the antiproton beam should be performed with help of the same hardware, as it is neither feasible nor cost-effective to reinstall and recommission the RF separation system between the different physics runs of AMBER. This implies that only one set of RF cavities can be installed with a frequency which must be able to satisfy the criteria for the purification of both particle species of interest, kaons and antiprotons.

Assuming that each group of cavities, RF1 and RF2, individually provides a kick resulting in a deflection angle θ, the total angle of RF kick θ_{tot}, by which the particle is deflected cumulatively in both RF1 and RF2, can be calculated as

$$\theta_{tot} = \theta\left(\sin(\varphi(t)) + \sin(\varphi(t) + \alpha)\right) = 2\theta \sin\left(\varphi(t) + \frac{\alpha}{2}\right)\cos\left(\frac{\alpha}{2}\right) \tag{3}$$

with $\varphi(t)$ being the phase of the particle in the RF wave of RF1 and α being the phase difference between RF1 and RF2. The maximum of $\frac{\theta_{tot}}{\theta} = 2$ is achieved if $\alpha = \pi$. However, since the particles are uniformly distributed along the phase of the RF cavities, the RMS deflection angle for a given particle type can be calculated as

$$\bar{\theta} = \sqrt{\frac{1}{2\pi}\int_0^{2\pi} \theta_{tot}^2(\varphi) d\varphi} = \sqrt{2}\theta \cos\left(\frac{\alpha}{2}\right) \tag{4}$$

For the case when positive kaons are the particle of interest, it is important to filter out the pions and protons, which respectively contribute to 50%–70% and 20%–30% of the overall beam intensity (dependent on the particle momentum). In order to filter them out effectively, one can adjust the frequency and particle momentum such that the phase difference between the protons and the positively charged pions (which is the same as for antiprotons and negatively charged pions) is $\Delta\varphi_{pion}^{antiproton} = 2\pi$. In that case, the phase difference between RF1 and RF2 for both of those particle types can be set to $\alpha = \pi$ and hence to propagate along the beam axis with $\theta_{tot} = 0$, while

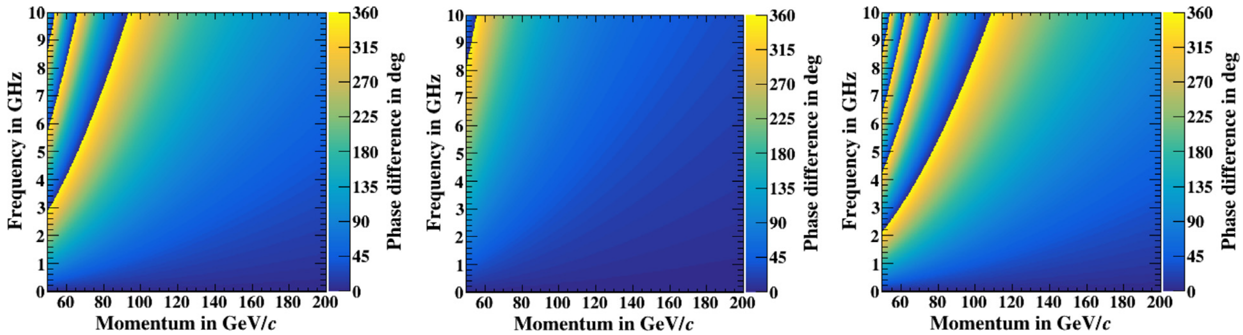

Fig. 4. Kaon–antiproton (left), pion–kaon (center) and pion–antiproton (right) phase differences as a function of particle momenta and RF-frequency.

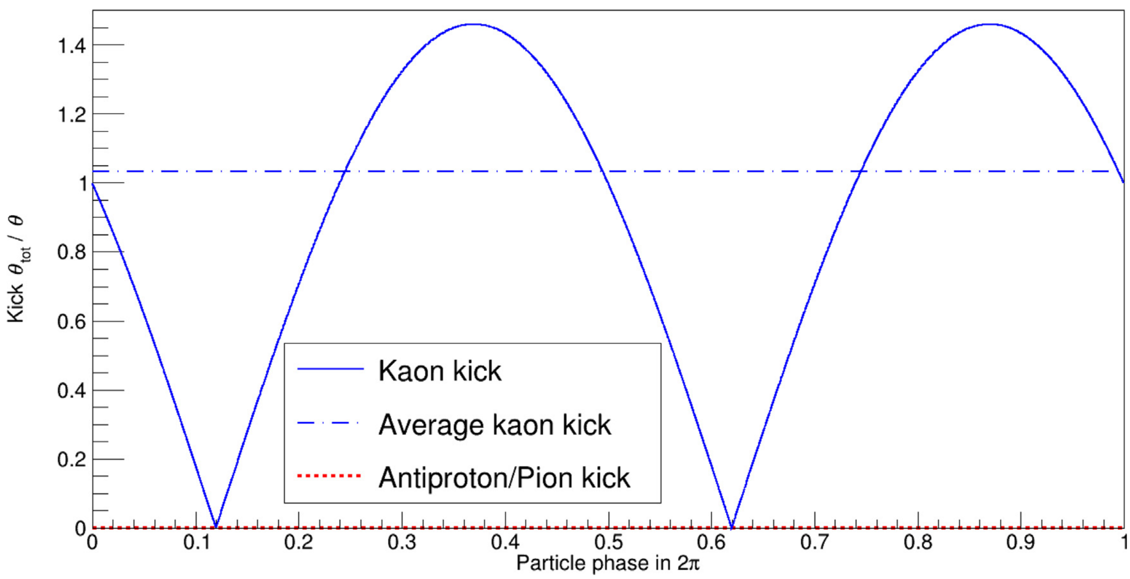

Fig. 5. Illustration of deflection of pions, antiprotons and kaons for $\Delta\varphi_{\rm pion}^{\rm antiproton} = 2\pi$.

the kaons receive a non-zero total deflection, as demonstrated in Fig. 5. Such setting of the phase difference limits the choice of frequency and momentum of the beam to the regions depicted with yellow color in Fig. 4, bottom. Depending on the choice of RF frequency in the cavities, described in the following chapters, the optimal momentum of the beam can be selected. As an example, Fig. 5 demonstrates the deflection of a beam with a momentum of 75 GeV/c and an RF frequency of $f \approx 4.72$ GHz, resulting in $\Delta\varphi_{\rm pion}^{\rm antiproton} = 2\pi$.

The same scheme cannot be used to deliver a purified antiproton beam, since for $\Delta\varphi_{\rm pion}^{\rm kaon} = 2\pi$ and for the momentum range of interest for AMBER (around 100 GeV/c) the frequency requirement on the RF cavity would become unrealistic, as it is demonstrated in Fig. 4, middle. Furthermore, since the cost of RF cavities is not negligible, it is envisaged to utilize the same hardware (and hence the same RF frequency) for the purification of the kaon and antiproton beams. Hence, another operation mode needs to be used: for the frequency $f \approx 4.72$ GHz one can achieve a phase separation of $\Delta\varphi_{\rm pion}^{\rm antiproton} = \pi$ for the beam momentum of 106 GeV/c. In that case the pions can be set to $\alpha = \pi$, so that they are dumped, while the antiprotons are maximally deflected and circumvent the dump most efficiently (see Fig. 6). The drawback of this operation mode is that the kaons are also somewhat deflected (although not by the same amount as antiprotons) and hence will not be completely filtered out. However, given their relatively small contribution to the beam intensity, still a significant antiproton beam purification can be achieved with this setting.

4. M2 beam line considerations

4.1. Different beam optics settings scenarios

The particles of any beam do not follow precisely the nominal path, but have some non-zero offsets from the nominal trajectory in space, direction and momentum. The transverse distribution of the beam is described by the emittance, which corresponds to the area that particles occupy in the transverse phase space. The emittance is conserved, unless the beam is being accelerated, decelerated, collimated or scattered (Liouville's theorem) [16]. The transport of the particles along the beam line can be described in first order by the linear algebraic approach with the transfer matrices [16]. Depending on the setting of the magnets, the beam can be focused or defocused at specific locations, or be directed parallel to the nominal trajectory. With respect to the RF separated beam of M2, two major options have been considered: one with the beam being focussed at the location of the cavities and one with a parallel beam in the cavities (see Fig. 7).

For the focused beam the beam size in the cavities is minimized. In this case, the R_{12} and R_{34} parameters of the aforementioned transfer matrices between the point-source-like T6 target and the center of the RF cavity locations RF1 and RF2 are set to zero. This means that the initial angle of particle propagation in the transverse beam planes X and Y does not influence the offset of this particle's position in the X and Y planes at the observed location. Also, the initial divergence of the beam, which is the major contributor to the beam size along the

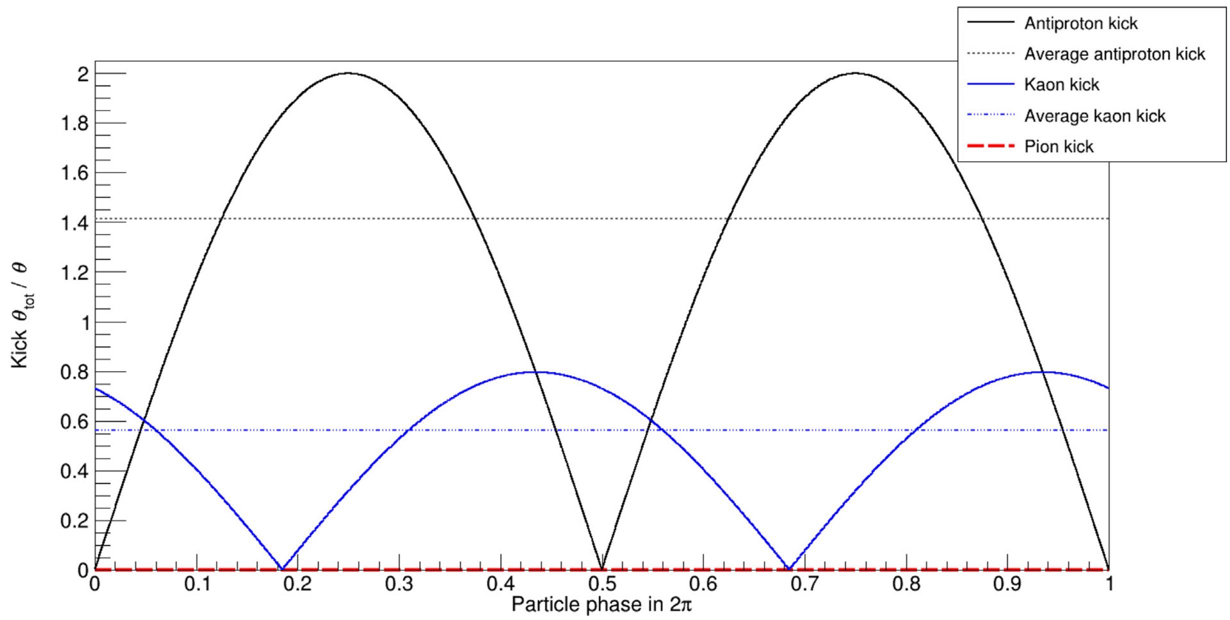

Fig. 6. Illustration of deflection of pions, antiprotons and kaons for $\Delta\varphi_{\text{pion}}^{\text{antiproton}} = \pi$.

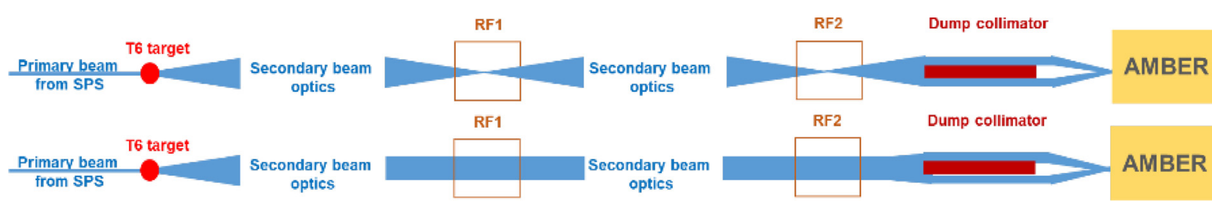

Fig. 7. Illustration of RF-separated beam optics with focused (top) and parallel (bottom) beam at the location of the RF cavities.

beam line, does not influence the beam size in X and Y at this specific location. Due to the emittance conservation, this implies that the phase space ellipse occupied by the beam is small in size X, but large in divergence X', as it is demonstrated in Fig. 8, top. The advantage of such setting is that the beam fits well through the aperture of the cavities, which might otherwise become a limiting factor for the transmission, as will be described below. The disadvantage of focused optics is that the relative kick provided by the cavities is small, so that the beam deflection is smaller than the divergence of the beam at this location. This means that after passing the cavities of this type, there would still be a large overlap between the deflected beam of wanted particles and the non-deflected beam of unwanted particles, resulting in a lower purity of the beam after the RF separation.

For the parallel beam the divergence of the beam in the plane of the RF kick (X in this specific design) in the cavities is minimized, implying that the R_{22} matrix parameter is zero at the location of the cavities. The beam size in the cavities is then determined by the angular acceptance of the beam line and the R_{12} parameter in the RF cavities, which, given the deflection requirements, have realistic radii up to 15 mm. Such a parallel beam is small in divergence X', but large in X (see Fig. 8, bottom). The downside of this configuration is that the transmission is strongly limited by the apertures of the RF cavities. Large losses at those superconducting cavities cannot be accepted, since they can cause quenches, and hence the beam would need to be pre-collimated. On the positive side, the relative effect of the RF kick is large, since the divergence of the beam is small which allows for a better separation of the wanted particles from the unwanted ones and hence this option is capable of providing a higher purity.

Both options, the focused and the parallel beam in the RF cavities, have been considered. Also, the beam has been made as parallel as possible at the location of the CEDARs to permit maximally effective particle identification. This is due to CEDARs being able to effectively identify particles propagating with less than 60 μrad to its axis. The beam optics were developed such that the momentum resolution stays below 1%. The distance between the two groups of cavities (RF1 and RF2) was maximized ($L \approx 830$ m), while maintaining the present geometry of the tunnel. The dump for the unwanted particles is located 20 m downstream of RF2 and is assumed to be 5 m long.

The purity and intensity of the beam are the crucial design goals for an RF-separated beam line. They depend on a number of beam line optics settings, such as (i) the transverse beam line acceptance determined by the first six quadrupoles in the upstream part of the beam line, (ii) the beam momentum spread, which impacts the differences in the time of flight of the particles, (iii) the magnification factor of the parallel beam set by the R_{12} parameter at the location of the RF cavities, and (iv) the RF cavity type, which determines the cavity kick, frequency, length and iris aperture.

4.2. Proposed beam line optics

The cavities assumed for the optics design are in accordance with the parameters of the crab cavities proposed for the ILC, having an RF frequency of 3.9 GHz, a deflection gradient of 5 MV/m, an iris size of d = 30 mm and a length of L = 10 m for each RF1 and RF2. These parameters are crucial to determine the possible beam size at the cavity, while one must take into consideration that the cavity does not only have to be able to permit the passage of undeflected beam, but also must contain the beam at the exit region of the cavity, which has already received the deflecting kick (see Fig. 9).

In the present design the beam is collimated upstream of RF1 to make sure that it fits well through the cavities, including its exit point. The width of the collimators is calculated as follows: Since the

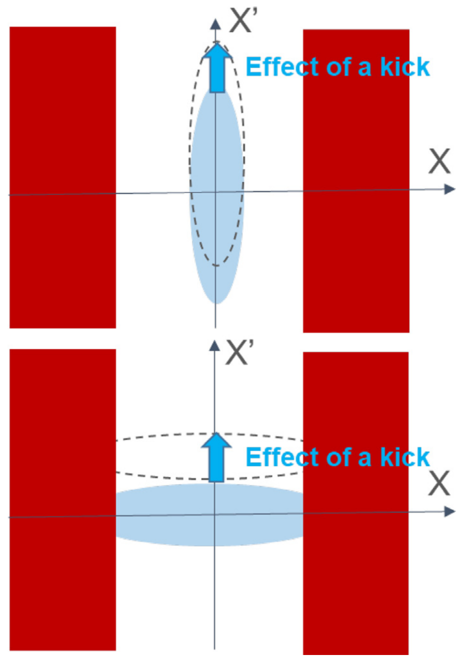

Fig. 8. Illustration of the focused (top) and parallel (bottom) beam passing through the apertures of the RF cavities (in red) and receiving the RF deflection kick (indicated with the blue arrow).

Fig. 9. Illustration of the beam (in blue) becoming wider during the propagation through an RF cavity (brown box) due to the RF deflection.

deflecting field is approximately homogeneous, the angle of the beam with respect to its propagation axis increases linearly in the cavities, i.e.

$$x'(z) = \frac{\frac{dp}{dz}}{p} \cdot z \tag{5}$$

with $\frac{dp}{dz}$ being the cavity gradient, p the beam momentum and z the coordinate along the beam line. The maximal size of the beam at the cavity exit can be obtained by integrating x' with respect to z, leading to

$$\sigma_x(z) = \frac{\frac{dp}{dz}}{2p} \cdot z^2 + \sigma_{x_0}, \tag{6}$$

with x_0 being the beam size at the cavity entrance and assuming that it is perfectly parallel. To get the beam through the cavity, it should be maximally as large as the cavity iris, i.e. $x(L) = \frac{d}{2}$. This imposes the following constraint on the collimator defining x_0:

$$x_0 = \frac{1}{2}\left(d - \frac{\frac{dp}{dz}}{p} \cdot L^2\right), \tag{7}$$

which leads to a collimator half-opening of about 11.5 mm for the given cavity parameters and a beam momentum of 68 GeV/c.

Based on this, one can simulate the RF separation. The following diagrams are always for a negative kaon beam at a central beam momentum of 68 GeV/c, meaning that the phase difference is tuned such a way that pions and antiprotons on average do not get a kick, while the kaons are deflected, as described above. For the current set of beam optics, the resulting angular distribution behind the second cavity is shown in Fig. 10.

One can clearly see that the wanted particles get an angular deflection different from 0, while the unwanted ones are efficiently filtered in terms of angle. The smearing of the distribution is caused by initial nonzero divergence of the beam as well as its finite momentum resolution.

The RF-separation technique filters out different species in terms of their angles with respect to the beam axis. Obviously though, when placing a dump in the beam one does not filter out by angle, but by position. Therefore, it is necessary to translate those angular differences in particle type specific distributions into positional differences. This can be done by a simple drift, as it is demonstrated via the phase space diagrams shown in Figs. 11 and 12.

At the cavity exit the spatial distributions fill out the whole cavity iris. As the kaons are the particles of interest, they have on average an angle different from zero leading to a shift of their spatial distribution, while the one for the pions will still be centered around zero after a certain drift. In the current optics design this drift is 20 m long.

In Fig. 12 the phase space after the 20 m long drift is shown. As expected, the pions are still located close to zero position in X-plane, while the position of kaons has changed due to the kick and subsequent drift. The two inner lines show an example of a beam dump, which is a vertical plate of material, the width of which in the X-plane (the plane of RF kick) can be modified. For a half-width of 20 mm this dump would absorb 59% of the kaons exiting RF2, but 92% of pions. The other two tilted lines indicate the aperture of the quadrupole behind the dump, refocussing the beam back towards the optical axis (this aperture limits the length of the drift from RF2 to the beam dump). The lines of its aperture are tilted, since the quadrupole is located downstream of the dump and hence further translation of the particle angle into the transverse position offset will take place between the dump and the quadrupole location.

4.3. Optimization of the RF separation

In this design one can tune the kaon purity and intensity by changing the width of the beam dump downstream of RF2. Clearly, by increasing the width, the purity would increase, but the beam intensity (for both wanted and unwanted components) would decrease. Conversely, by decreasing the dump width, one can increase the beam intensity by compromising beam purity. In Fig. 13 this interplay is shown for different optics settings at the cavity locations. The starting point of the optics development is represented by the green crosses. The settings of the beam line quadrupoles were adjusted to modify the beam optics to provide a focus in the cavities. This leads to a high total transmission and therefore a high beam intensity for the reasons illustrated in Fig. 8, top. But because of the focus, the relative effect of the cavity deflection is smaller, leading to an inability to obtain kaon purities over about 50%. With cavities having a larger iris size it is possible to go to a parallel beam inside the cavities increasing the relative effect of the kick. When aiming at highest purities it is therefore necessary to make the beam as parallel as possible. This option is represented by the blue circles in Fig. 13. There is a sharp drop of intensity at low purities, since the cavities have a finite iris and as long as the beam dump is smaller than the iris itself, one simply loses intensity without gaining much in terms of purity as all species are uniformly distributed over the cavity aperture. At higher purity levels the kaon intensity stays constant with increasing purity, as the angles of the different species are purely determined by the deflection and not by the intrinsic beam divergence. Unfortunately, the trade-off is a low overall intensity as the beam is large, leading to high losses at the collimator upstream of RF1.

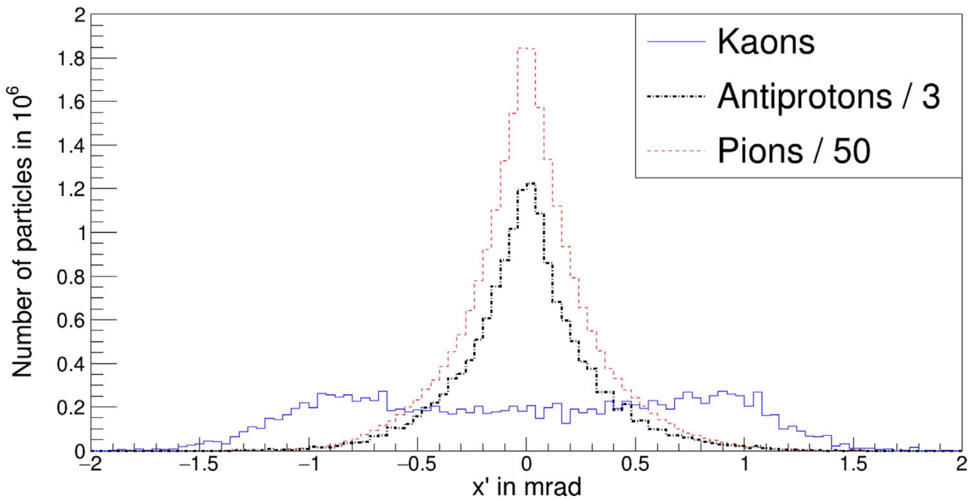

Fig. 10. Angular distribution behind RF2 for a kaon beam at 68 GeV/c. For a better display of the graph a renormalization was applied: The number of simulated pions was divided by 50, while the number of antiprotons was divided by 3.

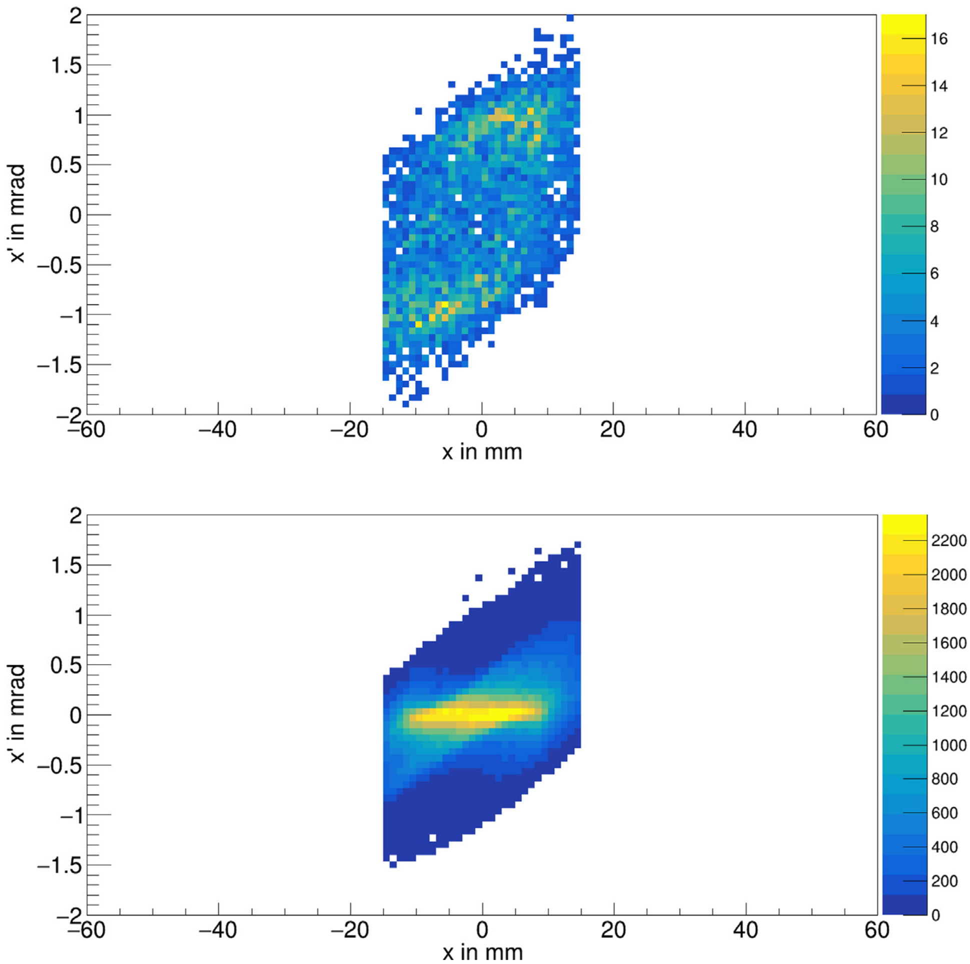

Fig. 11. Phase space of kaons (top) and pions (bottom) at the exit of RF2.

The ideal option is an optics setting reaching a high intensity at a high purity. This is achieved for a beam that is as parallel as possible while still fitting through the cavity. As the beam evolution in the deflection plane is dominantly determined by the R_{12}-term in the transfer matrices, the maximal value of it can be calculated by the iris size and the acceptance of the beam line in the deflection plane. Considering only the physical iris, this would mean the beam could be fully transported through the cavities for $R_{12} = 7.5$ mm/mrad. Taking into account the reduction of the effective usable iris size due to deflection described at the beginning of the present section, this reduces to $R_{12} \geq 5$ mm/mrad. A setting like this is less performant in terms of separation, but for the experiment it is important to still have a

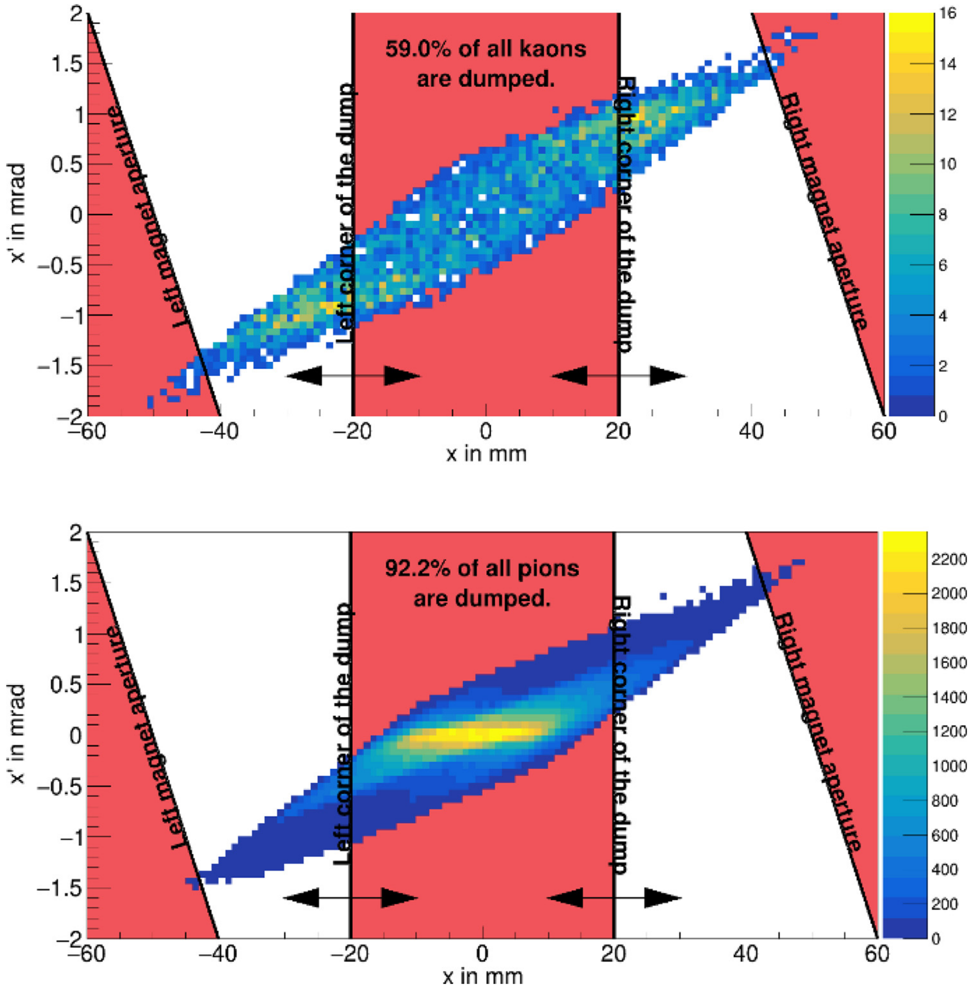

Fig. 12. Phase space of kaons (top) and pions (bottom) 20 m behind RF2. The red areas indicate the regions collimated by the dump or the magnet aperture.

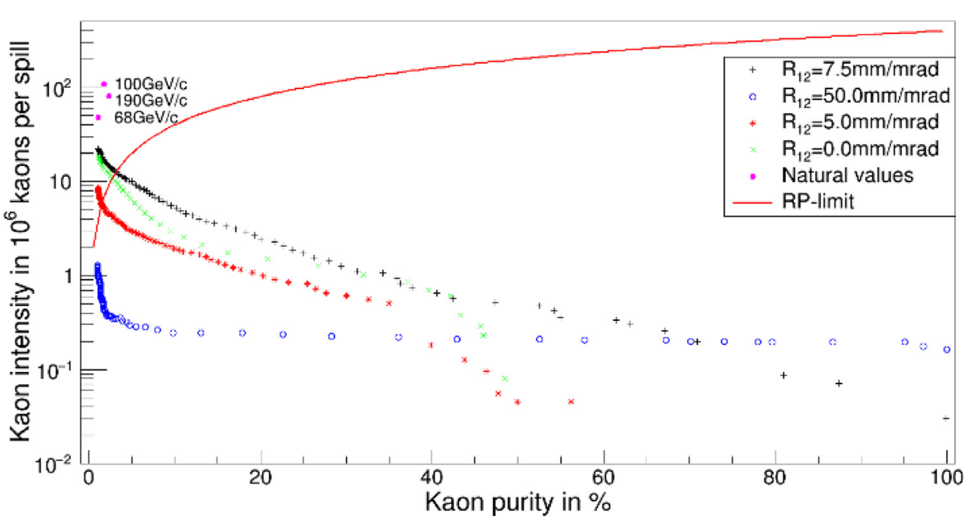

Fig. 13. Kaon beam intensity depending on the kaon purity for various optics settings. Red line signifies the limit imposed by Radiation Protection considerations for the maximal beam intensity in the EHN2 hall. Purple points represent the maximal intensities that could be delivered for the respective beam energies without the application of the RF separation technique. The other values represent the possible kaon intensity as a function of its purity for the different beam optics settings, such as focussed beam optics ($R_{12} = 0$) and various parallel beam optics options ($R_{12} \neq 0$).

Table 3
RF requirements.

Deflecting voltage per RF station	50 MV
RF Frequency range	Above 3 GHz
Spill length	4.8 s
Repetition rate	10 s–50 s
Beam aperture	~30 mm

high intensity at a reasonable purity. For that reason, the transmission along the whole M2 beam line has been optimized for the black crosses in Fig. 13. This can be seen in the fact that the total intensity for a parallel beam setting is higher than for the optics aiming at a focus in the cavities.

Considering the black crosses in Fig. 13, with the corresponding set of optics one is able to provide a kaon intensity of 10^6 per spill at the AMBER target of 40% purity. Allowing a lower purity of 20%, one can reach already a rate that is three times higher, i.e. $3 \cdot 10^6$ kaons per spill. In both cases, one would be far below the radio-protection limit shown (red solid curve in Fig. 13) in the experimental hall, where the AMBER experiment will be located.

Considering the RP-limit of $4 \cdot 10^8$ particles per spill, everything above the solid red curve would be too high intensity, meaning that the rate still would need to be decreased.

4.4. Conclusions from beam line optics examination

As indicated in Table 2, the required beam intensities for AMBER Phase-2 measurements of the kaon charge radius, the kaonic Primakoff reaction, kaon spectroscopy and prompt-photon production are in the order of 5 × 105 Hz or 105 particles per spill. As Fig. 13 indicates, the currently achieved beam intensity by RF separation should make it possible to reach the goals set for the aforementioned programs. The analysis of the expected efficiency of CEDAR detectors is not yet finalized and the optimization of it is ongoing, but the purity delivered by the RF separation technique seems to lie in the correct order of magnitude to comply with the requirements of AMBER after the selection of relevant particles by the CEDAR tagging. In contrast, the high beam intensities in the order of 10^8 particles per spill needed for the Drell–Yan studies cannot be provided with the RF-separation technique on the basis of the current radiation protection limitations, given the length of M2 beam line and the technical capabilities of the cavities. For this reason, the conventional M2 hadron beam is currently revised to improve the number of kaons reaching EHN2. As those are identified by Cherenkov counters before entering the hall, it is necessary to tag as many of them as possible. This, in turn, requires a more parallel beam at the CEDAR location, which is also under investigation at the moment.

5. RF cavities & RF power

As discussed in the sections above, the parameters of the RF-deflection system have a large impact on the performance of the RF-separated beam technique. Large deflecting voltage, large iris size, high RF frequency and low cost would be an ideal combination, but in reality these requirements are mutually in conflict and hence a compromise needs to be found. Different sets of requirements for the RF system have been considered, which led to the specifications summarized in Table 3. The frequency limitation is based on the beam momentum necessary for the AMBER physics program described in Section 2. The duration of the spill length and the SPS supercycle are the quantities determined by the duty cycle of SPS and its physics program, and hence the typical values from the recent decades of operation can be utilized. Finally, the deflecting voltage and the beam aperture values are close to the existing designs of the ILC crab cavities and are considered to be realistic [17].

5.1. Cavity requirements

In RF terms, a spill length of ~5 s means that the RF structures need to sustain the heat load of continuous wave (CW) operation. This excludes the use of normal conducting cavities as the deflection voltage per meter would have to be very low in order to reduce surface heating, thereby lengthening the RF sections to impractical values. Hence superconducting (SC) cavities are considered in the following, which have the additional advantage that larger apertures can be realized.

Deflecting cavities or crab cavities are typically used in colliders to reduce the loss of luminosity caused by the finite beam crossing angle at the collision. The International Linear Collider Study (ILC) considers 9-cell 3.9 GHz dipole cavities [17] for this purpose and here we use this design to estimate the number of needed cavities and the RF power (see Table 4). Using a realistic deflection voltage of ~2 MV/cavity and a total of 24 cavities provides 50 MV per RF station. As typical RF cryomodules contain around 8 cavities, M2 beam line would have three modules of ~6 m at each of the two RF stations, RF1 and RF2.

5.2. RF power

The RF power needed at the cavity input (P_{in}) is determined by the sum of the dissipated RF power on the cavity surfaces (P_{diss}), the beam loading (power given to the beam, P_b), and the power (P_{stab}) needed to stabilize the cavity frequency against small oscillations (Δ f) caused by microphonics. As the dissipated power (parameters see Table 4)

$$P_{diss} = \frac{V^2}{\left(\frac{R}{Q}\right) Q_0} \approx 6\,\mathrm{W} \tag{8}$$

and the power given to the beam [$O(\mu W)$] are negligible, the cavity RF input power is only determined by the constraints to keep the cavities on tune. In the above equation V stands for the deflecting voltage, (R/Q) is the figure of merit for the deflecting cavity mode, which depends only on the cavity geometry, and $Q_0 = \frac{\omega_0 W}{P_{Diss}}$ is the quality factor of this mode with the stored energy W and angular resonant frequency ω_0. The RF input power to keep the cavities on tune for maximum frequency deviations Δf is defined by [18]

$$P_{in} = \frac{V^2}{4(R/Q)Q_{ex}} \left(1 + \left(2Q_{ex}\frac{\Delta f}{f}\right)^2\right) \tag{9}$$

where all quantities are related to the dipole deflecting mode. Q_{ex} is defined as the quality factor of the "external load", meaning that if a cavity is switched off, part of its stored energy is dissipated through the power coupler towards the RF generator. This is characterized by the power $P_{ex} = \frac{V^2_{\{gen\}}}{2Z_0}$ with Z_0 being the impedance of the waveguide connecting power coupler and RF generator. Q_{ex} is then defined as $Q_{ex} = \frac{\omega_0 W}{P_{ex}}$. The loaded Q of the cavity-coupler ensemble is defined by $\frac{1}{Q_l} = \frac{1}{Q_{ex}} + \frac{1}{Q_0}$. In our case the dissipated power (and the beam power) is negligible in comparison to the power needed to stabilize the cavity, that means $Q_{ex} >> Q_0$, which basically means that (i) most of the incoming power is reflected back through the coupler, and (ii) that $Q_l \approx Q_{ex}$. Hence, we can use Eq. (9) to estimate an optimum Q_l to minimize the power consumption for a realistic maximum detuning (e.g. $\Delta f \leq 1\,\mathrm{kHz}$). At a $Q_l = 2 \times 10^6$ we find that ~5 kW per cavity are needed to keep the cavities on tune. It should be noted that a better frequency stabilization, e.g. to a level of $\Delta f \leq 100\,\mathrm{Hz}$, may be reached with a Ferroelectric Fast Reactive Tuner (FeFRT) [19], which would then reduce the power needs per cavity to less than 1 kW (at $Q_l = 1 \times 10^7$).

In order to reduce the cost of the RF power system it is recommended to choose RF sources that are readily available from manufacturers, such as klystrons or solid-state amplifiers. In the case of klystrons, the authors found one manufacturer that can supply 3 kW tubes operating at 3.9 GHz, which would be suitable for a frequency bandwidth slightly below 1 kHz.

Table 4
SC cavity parameters for AMBER, extrapolated from ILC Crab Cavities.

RF frequency (f)	3.9 GHz
Cells per cavity	9
Active length per cavity	0.34 m
Aperture radius	15 mm
Deflection	6.1 MV/m
Deflection per cavity (V)	2.08 MV
Cavities per RF station	24
Cavities per cryomodule	8
Cryomodules per RF station	3
Cryomodule length	~6 m
R/Q (transverse)	235 Ω
Q_0 @70 nΩ, 1.8K	3.2×10^9
Q_l (loaded Q for 1 kHz phase stabilization)	2×10^6
P_{in} (power needed at cavity input)	≤5 kW
Expected number of particles per spill passing through the cavities	$<1 \times 10^{10}$

5.3. RF conclusions

A draft layout for the RF system was made based on existing ILC cavity designs. At each of the 2 RF stations 3 cryomodules with 24 9-cell cavities will be needed to achieve 50 MV of deflecting voltage. This corresponds to ~20 m of beamline per station dedicated to RF cavities. The resulting set of parameters is summarized in Table 4. While all these values are achievable, all parameters (RF frequency, cryogenic temperature, cavity bandwidth, power needs, aperture, etc.) should be optimized to increase the particle yield and to reduce RF power consumption.

For the purpose of the aforementioned beam optics simulation it was assumed that the deflecting field is homogeneous across the complete aperture of the cavity. This assumption was necessary when using the simulation code MADX, deployed in the calculations described above, since this code does not permit simulation of transversely varying deflecting fields. It is a valid first order assumption in the center of the cavity (about 1 cm radius) [20]. This field deviation will introduce different field magnitude and direction at these locations, as well as the presence of higher order components. The effect of these variations is mitigated by the fact that the beam optics conditions are identical in RF1 and RF2 and there is a beam optics imaging between those locations. As a consequence, the particles pass through a similar transverse location in RF1 and RF2, and so the effect of the kick on the individual particle is the same in both cavities. The compensation of the kicks in the opposite directions for the particles designated to be dumped is therefore expected to function independent of the exact field distribution. However, the overall deflection angle θ_{tot} described in Eq. (3) could be impacted by those field variations for particles that are not designated for dumping and hence have a non-zero overall deflection.

In the medium-term, a thorough simulation of a cavity is required to establish a full 3D map of the oscillating deflecting field. Using the field from the simulation (e.g. with the BDSIM code [21]) will permit a more realistic calculation of the effect of the cavities on the deflection and distortion of the beam.

One potential optimization might include the circular polarization of the RF kick, hence providing deflection (and resulting particle purification) in both X and Y dimensions simultaneously. This option would require a recalculation of the beam optics and a redesign of the beam dump. If successful, it would also mitigate the problem of the transversely varying deflection field present in the dipole operation mode of the cavity, since the circularly polarized electric field is expected to vary less with azimuthal angle.

6. Summary

Phase-2 of the AMBER experiment, which is being proposed for operation at the M2 beam line of the CERN North Area complex, requires a higher intensity and purity of kaon (priority 1) and antiproton (priority 2) beams than currently delivered by the beam line. The share of kaons and antiprotons in the beam is limited by their production rate at the primary target and the kaon decay along the more than 1.1 km long beam line. Furthermore, the overall intensity of the beam is limited by radiation protection considerations in the EHN2 hall that is proposed to host the experiment.

The RF-separated beam technique is an option to increase the share of kaons and/or antiprotons in the M2 beam. Different beam optics settings have been examined and extensive tracking simulations have been performed, optimizing the beam intensity and purity of the potential RF-separated beam. This was done in close collaboration with the RF group at CERN and hence based on realistic expected parameters of the RF cavities.

No showstoppers have been identified for a possible RF-separated M2 beam to deliver the required intensities and purities for the envisaged AMBER Phase-2 measurements of kaonic Primakoff reactions, kaon spectroscopy, prompt-photon production and kaon charge radius. Hence it is foreseen to continue the feasibility and conceptual design study. Concerning the very high beam intensities required for the kaon-induced Drell–Yan data taking programme of AMBER Phase-2, however, it has been found that the RF-separated beam technique does presently not meet the expectations. Hence alternative scenarios for the improvement of particle identification by the CEDAR Cherenkov detectors need to be examined, which include the installation of additional vacuum, modification of beam optics and modifications of the CEDAR design.

Declaration of competing interest

The authors declare that they have no known competing financial interests or personal relationships that could have appeared to influence the work reported in this paper.

Data availability

Data will be made available on request.

Acknowledgments

The authors would like to warmly thank Alexej Grudiev, Walter Wuensch, Graeme Campbell Burt, Leo Bellantoni, Augusto Ceccucci and Marcia Quaresma for their contributions to the discussions on beam requirements and RF-cavity capabilities. The continuous support by Craig Roberts in developing the AMBER physics case is highly acknowledged.

References

[1] D. Banerjee, J. Bernhard, M. Brugger, N. Charitonidis, N. Doble, L. Gatignon, A. Gerbershagen, The North Experimental Area at the Cern Super Proton Synchrotron, CERN Document Server, CERN-ACC-NOTE-2021-0015, 2021.

[2] B. Adams, et al., COMPASS++/AMBER: Proposal for Measurements at the M2 Beam, CERN-SPSC-2019-022, SPSC-P-360, CERN, Geneva, 2019.

[3] H.W. Atherton, C. Bovet, N.T. Doble, L. Piemontese, A. Placci, M. Placidi, D.E. Plane, M. Reinharz, E. Rossa, G.V. Holtey, Precise measurements of particle production by 400 GeV/c protons on beryllium targets, CERN Yellow Reports: Monographs, CERN-80-07, CERN, Geneva, 1980.

[4] B. Adams, et al., Letter of Intent: A New QCD Facility At the M2 Beam Line of the CERN SPS (COMPASS++/AMBER), Tech. rep., CERN-SPSC-2019-003 (SPSC-I-250), 2019, arXiv:1808.00848.

[5] T. Horn, C. Roberts, The pion: an enigma within the standard model, J. Phys. G 43 (073001) (2016) 1–46.

[6] Perceiving the Emergence of Hadron Mass Through AMBER@CERN, 2021, [Online]. Available: https://indico.cern.ch/event/1063883/.

[7] C.D. Roberts, Perspective on the origin of hadron masses, Few Body Syst. 58 (2017) 1.

[8] C.D. Roberts, et al., Insights into the emergence of mass from studies of pion and kaon structure, Prog. Part. Nucl. Phys. (ISSN: 0146-6410) 120 (2021) http://dx.doi.org/10.1016/j.ppnp.2021.103883.

[9] RF-Separated Beams for Amber- Kick Off Meeting, CERN, 2021, [Online]. Available https://indico.cern.ch/event/1069879/.

[10] C. Adolph, et al., Measurement of the charged-pion polarisability, Phys. Rev. Lett. 114 (2015) 062002.

[11] M. Aghasyan, et al., Light isovector resonances in π-p→$\pi-\pi-\pi$+p at 190 GeV/c, Phys. Rev. D 98 (2018) 092003.

[12] P. Abbon, et al., The COMPASS setup for physics with hadron beams, Nucl. Instrum. Methods A 779 (2015) 69.

[13] Panofsky, W. Wenzel, Rev. Sci. Instrum. 27 (1956) 967.

[14] W. Panofsky, Experience with a microwave separator, in: L. Kowarski (Ed.), Proc. Int. Conf. on High Energy Accelerators and Instrumentation, CERN, 1959, pp. 428–431. P. Phillips, Rev. Sci. Instr. 32 (1961) 13.

[15] H. Grote, F. Schmidt, L. Deniau, G. Roy, The MAD-X Program (Methodical Accelerator Design) Version 5.02.08, User's Reference Manual, European Laboratory for Particle Physics, Geneva, Switzerland, 2016.

[16] E. Wilson, An Introduction to Particle Accelerators, Oxford University Press, Oxford, UK, 2001.

[17] C. Adolphsen, Design of the ILC Crab Cavity System, EUROTeV-Report-2007-010, 2007.

[18] J. Tuckmantel, Cavity-Beam-Transmitter Interaction Formula Collection with Derivation, CERN-ATS-Note-2011-002 TECH, Geneva, Switzerland, 2011.

[19] N. Shipman, Ferroelectric fast reactive tuner application for SRF cavities, in: Proceedings of 12th International Particle Accelerator Conference (IPAC), 2021.

[20] C. Adolphsen, et al., Design of the ILC Crab Cavity System, SLAC-PUB-12751, FERMILAB-TM-2388, EUROTEV-REPORT-2007-010, 2007.

[21] L.J. Nevay, et al., BDSIM: An accelerator tracking code with particle-matter interactions, Comput. Phys. Comm. 252 (2020) 107200, http://dx.doi.org/10.1016/j.cpc.2020.107200.